Cervical spinal cord DTI is improved by reduced-FOV with specific balance between numbers of diffusion gradient directions and numbers of averages.

Journal:	*American Journal of Neuroradiology*
Manuscript ID	AJNR-16-00163.R1
Manuscript Type:	Original Research
Classifications:	MR: diffusion tensor imaging < MR, Spine: advanced imaging techniques < Spine

ABSTRACT

Background and purpose: Reduced-FOV (r-FOV) DTI is appealing to explore the cervical spinal cord but the optimal set of parameters needs to be clarified. We hypothesized that NEX should be favored over number of diffusion gradient directions (NDGD) regarding the strong orientation of the cord in a single rostro-caudal axis.

Materials and Methods: Fifteen healthy people underwent cervical spinal cord MRI at 3T including an anatomical 3D-MERGE, high resolution full-FOV DTI with 3 NEX and 20 NDGD and five sets of r-FOV DTI differently balanced in terms of NEX/NDGD: (3/20), (5/16), (7/12), (9/9) and (12/6). Each DTI sequence lasted 4m30s, an acceptable duration, to cover C1 to C4 in axial plane. FA maps and tractograms were reconstructed. Qualitatively, two radiologists rated the DTI sets blinded to the sequence. Quantitatively, we compared distortions, SNR, variance of FA values and numbers of detected fibers.

Results: Qualitatively, r-FOV DTI sequences with 5 NEX or more were significantly better rated than the f-FOV and the r-FOV using low NEX (n=3) and high NDGD (n=20). Quantitatively, the best tradeoff was reached by the r-FOV DTI with 9 NEX and 9 NDGD, which provided significantly less artifacts, higher SNR on trace b750, and increased number of fibers tracked while maintaining similar FA values and dispersion.

Conclusion: Optimized r-FOV DTI improves spinal cord imaging. The best compromise was obtained with 9 NEX and 9 NDGD which emphasizes the need for increasing NEX at the expense of NDGD for spinal cord DTI contrarily to brain DTI.

ABBREVIATIONS

CSC = cervical spinal cord; f-FOV = full FOV; FA = fractional anisotropy; MERGE = multiple echo-recombined gradient echo; NDGD = number of diffusion gradient directions; r-FOV = reduced FOV

KEY WORDS

Reduced field-of-view, cervical spinal cord, diffusion tensor imaging, quality control

INTRODUCTION

Cervical spinal cord (CSC) assessment on clinical daily routine still essentially relies on qualitative evaluation of conventional MRI sequences. Nonetheless, additional sequences could provide more sensitive information about CSC alterations notably in inflammatory, traumatic and neurodegenerative diseases[1-5]. Among them, diffusion tensor imaging (DTI), classically based on single-shot echo-planar-imaging (SS-EPI), could provide valuable qualitative information and quantitative surrogate biomarkers.

While DTI has been widely investigated in brain, its use for CSC imaging is still challenging and only restricted to preclinical and monocentric clinical studies. There are several reasons for these limitations including the facts that CSC is a small structure, prone to distortions, susceptibility artifacts especially with long echo planar readout train, flow artifacts and physiologic motion artifacts.

Among the various methods that have been implemented on MR-system to improve DTI image quality, reduced field-of-view (r-FOV) is particularly promising. It consists in reducing the FOV in the phase or frequency encoding direction in order to shorten the echo planar

readout train and attenuate susceptibility-and motion-related artifacts[6-11]. As the CSC is a small longitudinal structure, r-FOV is especially suitable for its exploration. One of the r-FOV techniques uses a 2D echo-planar radio frequency pulse to excite a rectangular-shaped FOV, with contiguous multi slices. K-space is then more rapidly acquired for the same spatial resolution, which decreases SS-EPI artifacts together with inherent fat-suppression[6].

On qualitative analysis, this CSC r-FOV diffusion-weighted imaging (DWI) method obtained from 3 orthogonal diffusion gradient directions has already demonstrated its ability for a better detection of anatomical details, with less ghosting and blurring artifacts[12], while apparent diffusion coefficient values were stable compared with conventional full-FOV CSC DWI (f-FOV).

However, there is no recommendation regarding the optimal set of parameters to perform r-FOV DTI in CSC. Some consensus has been reached (regarding the b-value, the voxel size, the number of excitations (NEX), the number of diffusion gradient directions (NDGD), and the bandwidth[13]) but these recommendations concern f-FOV DTI with parallel imaging, whose sequence scheme is different from the r-FOV scheme. The smaller voxel size that goes with r-FOV inherently leads to a decrease of signal-to-noise ratio (SNR). Classical strategies to recover SNR consist of increasing the NEX and/or the NDGD. Unlike brain DTI for which the NDGD should be privileged to the detriment of the NEX, to handle with the complex fiber orientation, there is no consensus about the best pair of NEX-NDGD for CSC DTI. One might even hypothesize that the best tradeoff of NEX-NDGD could be obtained by favoring NEX (unlike for brain-DTI) because the CSC is particularly affected by artifacts and basically presents one single prominent orientation. It is difficult to rely on phantom studies or theoretical analyses for such optimization in the CSC that could not take into account CSF pulsations, heartbeats or patient respiratory motions.

Therefore, the purpose of this study is to compare different sets of r-FOV CSC DTI depending on different pairs of NEX and NDGD and a standard f-FOV DTI. To do so, we used an empirical non-sequential optimization approach in which both NEX and NDGD were modified simultaneously with the only constraint of maintaining the same clinically acceptable scan duration. To evaluate image quality, we propose a practical clinical approach using a standardized test-bench for qualitative and quantitative evaluations derived from regions of interest and tractography.

MATERIALS AND METHODS

Patient population

15 healthy volunteers (six women, nine men; age range 22-30 years) were prospectively included after written informed consent was obtained. This study was approved by the local ethics committee review board.

Imaging Methods

All scans were performed on a 3Tesla MR scanner (Discovery MR750W, General Electric Healthcare®, Milwaukee, Wisconsin) equipped with high-performance gradients (maximum slew rate of 200 mT/m/ms and maximum strength of 44 mT/m) and using dedicated posterior coil with 40 elements and 19-channel phased array head neck spine coil.

Subjects were asked to breathe normally and not to swallow or cough during the acquisition. They were installed with a slight flexion of the head and with contentions in order to reduce involuntary movements.

All the sequences were performed in the axial plane with anterior-posterior phase-encoding direction and were prescribed with similar geometry in order to perform fair comparisons. Pulse triggering was not used to limit the scan time.

Conventional imaging. The protocol included an anatomical sagittal T2-weighted spin-echo and a 3D multiple echo-recombined gradient echo (MERGE) acquired in the same axial plan as DTI sequences (*i.e.* perpendicular to the long axis of the upper cervical spine). 3D-MERGE provides good white and gray matter differentiation with good SNR and was considered as the anatomical reference. 108 slices with resolution of 0.8×0.8×0.8 mm^3 covering a 140×140 mm^2 FOV were acquired in 8 minutes. Other sequence parameters were, TR/TE (10/5ms), flip angle 7°, turbo factor 36.

f-FOV DTI. Conventional CSC DTI corresponded to the DTI usually performed at our institution[14] which has been optimized beforehand according to the literature[15,16]. Parallel imaging was used (array spatial sensitivity encoding technique, ASSET) with an acceleration factor of 2. The SS-EPI parameters were: NDGD = 20 directions, b=0 s/mm² and b=750 s/mm², matrix = 96 x 96, FOV = 120 x 120mm², in plane resolution = 1.25 x 1.25 mm², slice thickness = 5 mm, TR/TE = 5600ms/75ms, and NEX = 3. This sequence covered CSC from C1 to C7 within 6m50s.

r-FOV DTI. For each subject, r-FOV DTI images were acquired by using 5 schemes with different combinations of NDGD and NEX for each direction, starting from a sequence with many directions (NDGD=20) and few excitations (NEX=3) up to an opposite scenario obtained with the minimum number of directions to calculate a diffusion tensor (NDGD=6) and a maximum number of excitations (NEX=12). Each scheme lasted about 4m30s to cover the upper cervical spine from C1 to C4. The 5 schemes of SS-EPI sequence were as follow in terms of NEX/NDGD: 3N/20D, 5N/16D, 7N/12D, 9N/9D, 12N/6D.The directions were non

collinear and generated according to the recommendations of DK Jones et al. for optimization of gradient vector orientations[17]. TR/TE were: 3600/75ms. The other parameters were fixed and corresponded to those applied for the f-FOV sequence in order to compare r-FOV and f-FOV, notably regarding voxel size (r-FOV was 96 × 48 with a matrix of 120 × 60 mm², in plane resolution = 1.25 × 1.25 mm², and 5mm slice thickness).

The entire protocol was performed during the same session and lasted 40 minutes.

Post-processing. Because our goal was to identify the best set of parameters for a DTI sequence to be used for clinical applications, we post-processed the images with the tools that are accessible on clinical systems. Therefore, the DTI dataset processing and the qualitative and ROI-based analyses were performed on GE Healthcare® AW server Workstation 5. Tractography-based analyses were performed with Oleasphere software (Olea Medical®, La Ciotat, France; www.olea-medical.com).

All the raw images were corrected for motion artifacts and eddy current distortion (ECC) with the same algorithm implemented on the GE Healthcare® DTI analysis software.

Radiological assessment (Figure 1)

Qualitative analysis. Two radiologists (A.C. and N.A. with respectively 4 and 7 years of experience in MRI) randomly evaluated the quality of each of the 6 DTI sequences (f-FOV, r-FOV 3N/20D, r-FOV 5N/16D, r-FOV 7N/12D, r-FOV 9N/9D, r-FOV 12N/6D) blinded to the nature of the sequence. They attributed a score based on a 4-point scale as follows, adapted from Zaharchuk *et al.*[12] 1 = non diagnostic, 2 = poor, 3 = moderate, 4 = good. This score was based on anatomical details, artifacts, distortion and perceived SNR from fractional anisotropy (FA) maps alone and fused with the 3D-MERGE. In case of disagreement between the two radiologists, consensus was obtained after discussion with a third experienced neuroradiologist (T.T with 14 years of experience).

Number of slices with artifacts. The number and the types of artifacts or non-diagnostic slices for each DTI sequence (flow artifact, motion artifact, susceptibility artifact, major distortion) were reported and expressed as the percentage of slices with artifacts out of the total number of slices.

Quantitative comparisons of FA values based on ROI analysis. For this part of the study, one neuroradiologist (A.C.), still blinded of the sequence, manually delineated ROIs on four slices passing through the middle of vertebral bodies C1, C2, C3 and C4. ROIs were positioned twice with good reproducibility (intraclass correlation = 0.788, $IC_{95\%}$ = [0.353;0.943])

Measurements were obtained on : (i) gray matter: left and right anterior horn of the cord (GM), (ii) white matter: left and right cortico-spinal tract (WM), and (iii) full section of the cervical spinal cord. ROIs were initially placed on the axial 3D-MERGE and then propagated on coregistered FA map. If needed, ROIs were slightly manually adjusted to account for FA map distortion. Because of partial volume effect at the interface between CSF and spinal cord with about 2 pixels showing intermediate FA values, measurements on the full section of the spinal cord were conducted on a smaller ROI eroded by 2 pixels. The FA values of each ROIs were extracted, right and left measurements being averaged (Figure 1.B) .

(i) Quantifications of residual distortion: The residual distortion after Eddy current correction was quantified by a ratio that we called "distortion ratio" and that was calculated as follow: Distortion ratio = $\frac{\left|(S_{(\text{Full Section - merge})} - S_{(\text{Full section - FA})}\right|}{S_{(\text{Full Section - merge})}} \times 100$

where S is the surface of the full section of the cervical spinal cord. Distortion ratio was calculated at the four cervical levels and then averaged to obtain one single distortion ratio value per patient for each sequence. It ranges from 0 when there is no distortion in the FA

map compared with the reference anatomical MERGE sequence and it increases when distortions are more pronounced.

(ii) Signal to noise ratio (SNR): Because multichannel coil and parallel imaging were used to collect DTI data, SNR cannot be exactly assessed[18]. In addition, background noise was not always included within the r-FOV DTI acquisition. So, we estimated spinal cord SNR at b0 and b=750s/mm² as the ratio between the signal of the full section of the cord and the standard deviation measured within the same neck muscle (longissimus capitis). SNR_{b0} and SNR_{b750} were assessed at the four cervical levels and then averaged in order to obtain a single SNR_{b0} and SNR_{b750} values per patient and per DTI sequence.

(iii) Variability of FA measurements: As a current issue with CSC DTI is its lack of precision and its variability even among healthy subjects, we aimed at estimating inter healthy volunteer variations. For this purpose, we measured FA on the full section, WM and GM at the four levels, and we calculated the mean and standard deviation of these four values.

Quantitative comparisons based on tractography analysis. Raw data were post processed with Oleasphere software®. Motion correction was performed. We drew two seed ROIs that included the entire section of the spine at C1 and C3 levels. We measured the number of fibers detected between these two ROIs, per patient and per DTI sequence. The following parameters were used for stopping the tractography: FA minimum = 0.25, maximum angle = 41.4°, fiber minimum length = 20mm

Statistical analyses

All statistical analyses were performed with Graphpad PRISM ® version 6. Gaussian distributions were tested with a Shapiro-Wilk normality test. For qualitative assessment, distortion ratio, SNR_{b0}, SNR_{b750}, mean FA values per topography and number of detected fibers by tractography, we used one way ANOVA (with post hoc t-test) or Kruskall-Wallis

(with post hoc Dunn test) depending on the distribution of the variables. For artifacts comparisons, contingency tables were built and we compared sequences with Fisher exact test to account for the small size of the sample. We performed Bartlett test to assess if the FA values of each DTI set have equal variance, after verification of Gaussian distribution. $P<0.05$ was deemed significant.

RESULTS

No incidental pathological finding was observed in these young subjects, notably, no degenerative disk disease.

Qualitative analysis

Figure 2 shows the superposition of FA map with the anatomical reference 3D-T2-MERGE at the four levels of interest (C1 to C4) and a sagittal reconstruction, for the f-FOV and the five r-FOV schemes, with the same FA color-scale.

On qualitative radiological assessment, the 4 r-FOV DTI sequences with 5 NEX or more were not scored differently from each other but were significantly better evaluated than the f-FOV images (3N/20D) (1.1±0.8) or the r-FOV 3N/20D (1.8±0.56) . There was no qualitative difference between the f-FOV sequence and the r-FOV 3N/20D sequence (Figure 3).

In detail, the two radiologists consistently observed fewer distortions, less misregistration in the anterior-posterior direction and less blurring for the r-FOV sequences with more than 5 NEX than for the 2 other sequences. The r-FOV images obtained with 5N/16D, 7N/12D, 9N/9D and 12N/6D provided CSC morphology closer to the anatomical reference as opposed to the f-FOV or the r-FOV 3N/20D images (Figures 2 and 3).

Number of slices with artifacts

The dataset with the highest number of slices with artifacts was the r-FOV 3N/20D (31.6%) followed by the f-FOV (22.7%) while the r-FOV sequences with 5 NEX or more were significantly better; the r-FOV 9N/9D being the one with the smaller amount of artifacts (13.3%) (Figure 4)

Artifacts were mainly due to CSF flow on b0 images and residual distortions after eddy current correction (this one especially for f-FOV and r-FOV 3N/20D), notably at the lower lever of the acquisition volume (C4).

Quantitative comparisons based on ROI analysis

The distortion ratio decreased continuously while increasing the NEX (and in turn decreasing the NDGD) even though this effect did not reach statistical significance (Figure 5.A). Thus, the distortion ratio for r-FOV 3N/20D and r-FOV 12N/6D were 13.14±6.6% and 9.25±5.5%, respectively.

SNR on b0 map did not exhibit significant difference between the sequences ($p>0.05$). At b=750mm²/s, no significant difference was observed between the DTI sets, except for the comparison between r-FOV 3N/20D and r-FOV 9N/9D, which had respectively the lowest and the highest SNR (23.95 ± 4 versus 36.04 ± 5.8, $p=0.0182$)(Figure 5.B). Considering that a critical threshold of SNR below 8 should lead to slice rejection, 10% of the slices had to be rejected because of a signal below this threshold on f-FOV, 6.7% on r-FOV 3N/20D, 5 % on r-FOV 7N/12D and r-FOV 12N/6D. SNR was always above 8 for r-FOV slices acquired with 5N/16D and with 9N/9D.

Whatever the location (full section, GM and WM) and whatever the sequences, comparisons of the distributions of FA values did not reveal significant difference (Figure 5.C).

Furthermore, there was no significant difference between the FA values depending on the acquisition pulse sequence. For instance, FA values of the full section was: 0.70 ± 0.04 for f-FOV, 0.74 ± 0.04 for r-FOV 3N/20D, 0.71 ± 0.05 for r-FOV 5N/16D, 0.7 ± 0.04 for r-FOV 7N/12D, 0.074 ± 0.03 for r-FOV 9N/9D and 0.74 ± 0.04 for r-FOV 12N/6D. The FA values that we obtained were consistent with the literature[19-22], with lower and more dispersed measures within GM, and higher and less dispersed measures within WM.

Quantitative comparisons based on tractography analysis

Figure 6.A represents tractograms derived from the two seeds superimposed on the corresponding trace b750. R-FOV 7N/12D, 9N/9D and 12N/6D qualitatively exhibited a more realistic anatomy of the cord than f-FOV, r-FOV 3N/20D and r-FOV 5N/16D with more fibers and longer tracts.

Quantitatively, r-FOV 9N/9D detected the highest number of tracts without abnormal tract findings on tractograms (4587 ± 1743), closely followed by r-FOV 12N/6D (4290 ± 1206) which was not significantly different from the previous. The best sequence (r-FOV 9N/9D) detected significantly more fibers than f-FOV ($p<0.0001$) r-FOV 5N/16D ($p=0.0004$) and r-FOV 3N/20D ($p<0.05$) (Figure 6.B).

DISCUSSION

Our study did not show any significant difference between CSC DTI obtained with f-FOV or r-FOV when using a protocol favoring NDGD over NEX. However, we showed real benefits of the r-FOV by balancing the NDGD and the NEX, the best tradeoff being 9N/9D, in terms of qualitative aspects, reduction of artifacts, SNR, and detection of fibers, while maintaining identical FA values.

This study demonstrates that optimized parameters for CSC DTI in clinical conditions are different from those for brain DTI that requires a high number of directions, ideally at least 31, while NEX can be reduced[23]. Here, we demonstrated that CSC DTI do not require such a high number of gradient directions. In theory, high NDGD leads to more precise DTI information. In the CSC, FA values and their variations were similar with 6, 9, 12, 16 or 20 NDGD in a set of healthy subjects which might be explained by the strong orientation of the cord in rostro-caudal axis. However we recommend increasing the number of averages as CSC presents low intrinsic signal and is prone to artifacts that can be averaged and canceled (such as flow artifacts) with several excitations. Altogether, we recommend privileging NEX over NDGD when time is limited as opposed to standard recommendation for brain exploration. These results might be particularly important when axial slices are used because axial is prone to flow artifacts. Other strategies could be adopted and associated in the future to further limit the flow artifacts: (i) many b0 could be acquired in order to select the one with the least artifacts, (ii) cardiac gating could be added but at the cost of increasing scan time (iii) averaging of two b0 acquisitions, in phase and in reversed phase and (iv) tensor could be estimated from b=50s/mm² and b=750s/mm² acquisition without requiring b0.

In line with this conclusion, previous studies dealing with the optimization of DTI parameters for CSC have also demonstrated, in a similar sequential approach, that there was no need to drastically increase NDGD (15 was satisfying when compared with 32) while NEX had to be boosted[13]. But these results were obtained with f-FOV sequence and we highlight here their relevance that might be still more important with a r-FOV strategy.

Other kinds of r-FOV sequences exist, depending on the MRI system, but all of them rely on the same principle. Reducing the excited region in the phase encoding direction enables shorter echo train, increased blip moment and thus reduced susceptibility effect[24] . Spatial definition can be improved. SNR and scan time are supposed to remain stable. Among the r-

FOV method, the most popular are: (i) ZOOM-EPI[11], an inner volume technique, in which a refocusing pulse in an orthogonal or oblique plane to the excitation plane is applied, but with creation of slice gaps, (ii) inner volume excitation and outer volume suppression[10] and (iii) the r-FOV [6]. As a consequence of the increased image quality, applications of r-FOV sequences are increasing not only for the CSC but also to explore midbrain, optic nerves, or hippocampi for neuroradiology, and also pancreas and prostate[25-26].

Currently, there is no validated method for CSC DTI quality control. CSC and its environment are too complex for mathematical[15] or phantom simulations. The method that we proposed here can be viewed as a realistic bench test that can be performed by any radiologist and that covers all the aspects of quality control.

Finally, we can expect further improvements as additional techniques are being developed: (i) the combination of parallel imaging and r-FOV, that has already been performed for the pons at 7T[27], can still increase DTI quality, (ii) multi segmented 3D-EPI could increase SNR and could be associated with r-FOV and parallel imaging to reduce echo train[28], (iii) more accurate diffusion model could be used such as NODDI[29] that might provide more accurate quantitative diffusion metrics especially for anisotropic structure like gray matter, (iv) improved post processing methods are being developed[30] with improved eddy-current and motion corrections.

Our study is not without limitations. We did not investigate other important parameters such as b-value, slice thickness, bandwidth, cardiac gating, respiratory gating and different design of diffusion vectors. But these parameters were set whatever the sequence. The values that we used range amongst those classically recommended[31], notably by MR constructors. Furthermore, all our acquisitions were performed on the same 3T MR-system. Further studies are required to investigate whether our results could be translated to 1.5T. The current

literature suggests that 1.5T and 3T should provide similar DTI results although a direct comparison hasn't been conducted for CSC DTI. Phantom studies with classical diffusion have shown that the increased SNR inherent at higher magnetic field was counterbalanced by increased distortions or susceptibility artifacts[32]. For brain DTI, Grech-Sollars et al. recently concluded that no significant difference was observed in the inter-scanner coefficient of variation for MD and FA when 1.5T and 3T systems were compared, with similar brain DTI protocols[33]. Therefore the parameter adjustments that we suggest at 3T might translate to 1.5T but a formal comparison will be needed to validate this statement. In addition, our patient population only consisted in healthy young adults without significant medical history, which might have led to better quality than what can be encountered in clinical routine. It is also admitted that degenerative, inflammatory, traumatic, metabolic or tumoural spinal diseases can modify diffusivity parameters[1-5]. Consequently, even though our study design allowed comparing the DTI sequences, the values of our judgement criteria cannot be translated directly in clinical practice. Another limitation of our study is that we only studied 15 healthy subjects, which might not be enough to have statistical power to detect subtle differences. Nonetheless, this sample already enabled to argue for a better set of parameters, namely r-FOV 9N/9D.

CONCLUSION

R-FOV CSC DTI is clinically feasible and provides significant qualitative and quantitative improvement when optimized. Contrarily to brain imaging, we recommend to limit NDGD and to increase NEX as CSC is a small strongly oriented structure generating low signal and subject to artifacts. The best compromise in a clinically acceptable scan time of 4m30s is r-FOV with 9 NEX and 9 NDGD.

Acknowledgements: We thank Marion Uettwiller, MR zone clinical leader for GE Healthcare; and Gerard Raffard for their implication in this study.

Funding: The work was supported by public grants from the French Agence Nationale de la Recherche within the context of the Investments for the Future program referenced ANR-10-LABX-57 named TRAIL and ANR-10-LABX-43 named BRAIN.

Paper previously presented in part at: Annual Meeting of the French Society of Radiology (Société française de radiologie), October 19, 2014, Paris, France; and Annual Meeting of the French Society of Neuroradiology (Société française de Neuroradiologie), April 8, 2015, Paris, France

REFERENCES

1. Shanmuganathan K, Gullapalli R, Zhuo J, et al. Diffusion Tensor MR Imaging in Cervical Spine Trauma. *American Journal of Neuroradiology* 2008;29:655–9.

2. Facon D, Ozanne A, Fillard P, et al. MR diffusion tensor imaging and fiber tracking in spinal cord compression. *AJNR Am J Neuroradiol* 26:1587–94.

3. Renoux J, Facon D, Fillard P, et al. MR diffusion tensor imaging and fiber tracking in inflammatory diseases of the spinal cord. *AJNR Am J Neuroradiol* 2006;27:1947–51.

4. Hecke W, Nagels G, Emonds G, et al. A diffusion tensor imaging group study of the spinal cord in multiple sclerosis patients with and without T2 spinal cord lesions. *J Magn Reson Imaging* 2009;30:25–34.

5. Budzik J-F, Balbi V, Thuc V, et al. Diffusion tensor imaging and fibre tracking in cervical spondylotic myelopathy. *Eur Radiol* 2010;21:426–33.

6. Saritas E, Cunningham C, Lee J, et al. DWI of the spinal cord with reduced FOV singleshot EPI. *Magn Reson Med* 2008;60:468–73.

7. Kim T, Zollinger L, Shi X, et al. Quantification of Diffusivities of the Human Cervical Spinal Cord Using a 2D Single-Shot Interleaved Multisection Inner Volume Diffusion-Weighted Echo-Planar Imaging Technique. *American Journal of Neuroradiology* 2009;31:682–7.

8. Finsterbusch J. High-resolution diffusion tensor imaging with inner field-of-view EPI. *J Magn Reson Imaging* 2009;29:987–93.

9. Jeong E, Kim S, Guo J, et al. High-resolution DTI with 2D interleaved multislice reduced FOV single-shot diffusion-weighted EPI (2D ss-rFOV-DWEPI). *Magn Reson Med* 2005;54:1575–9.

10. Wilm BJ, Svensson J, Henning A, et al. Reduced field-of-view MRI using outer volume suppression for spinal cord diffusion imaging. *Magn Reson Med* 2007;57:625–30.

11. Wheeler-Kingshott C, Hickman S, Parker G, et al. Investigating cervical spinal cord structure using axial diffusion tensor imaging. *Neuroimage* 2002;16:93–102.

12. Zaharchuk G, Saritas E, Andre J, et al. Reduced field-of-view diffusion imaging of the human spinal cord: comparison with conventional single-shot echo-planar imaging. *AJNR Am J Neuroradiol* 2011;32:813–20.

13. Lee J, Kim J, Kang H, et al. Optimization of acquisition parameters of diffusion-tensor magnetic resonance imaging in the spinal cord. *Invest Radiol* . 2006;41:553–9.

14. Crombe A, Menegon P, Tourdias T, et al. Diffusion tensor imaging of cervical spinal cord at 3T: normal values of radial, axial, mean diffusivities and fractional anisotropy in anterior horn, dorsal funiculus and pyramidal tract at each cervical level. *Proc Intl Soc Mag Reson Med (ISMRM)* 2014

15. Gao W, Zhu H, Lin W. A unified optimization approach for diffusion tensor imaging technique. *Neuroimage* 2008;44:729–41.

16. Mukherjee P, Chung S, Berman J, et al. Diffusion tensor MR imaging and fiber tractography: technical considerations. *AJNR Am J Neuroradiol* 2008;29:843–52.

17. Jones DK, Horsfield MA, Simmons. Optimal strategies for measuring diffusion in anisotropic systems by magnetic resonance imaging. *Magn Reson Med* 1999;42:515–25.

18. Dietrich O, Raya J, Reeder S, et al. Measurement of signal-to-noise ratios in MR images: Influence of multichannel coils, parallel imaging, and reconstruction filters. *J Magn Reson Imaging* 2007;26:375–85.

19. Brander A, Koskinen E, Luoto T, et al. Diffusion tensor imaging of the cervical spinal cord in healthy adult population: normative values and measurement reproducibility at 3T MRI. *Acta Radiologica* 2013;55:478–85.

20. Xu J, Shimony J, Klawiter E, et al. Improved in vivo diffusion tensor imaging of human cervical spinal cord. *Neuroimage* 2012;67:64–76.

21. Tang L, Wen Y, Zhou Z, et al. Reduced field-of-view DTI segmentation of cervical spine tissue. *Magn Reson Imaging* 2013;31:1507–14.

22. Ellingson B, Ulmer J, Kurpad S, et al. Diffusion tensor MR imaging of the neurologically intact human spinal cord. *AJNR Am J Neuroradiol* 2008;29:1279–84.

23. Ni H, Kavcic V, Shu T, et al. Effects of number of diffusion gradient directions on derived diffusion tensor imaging indices in human brain. *AJNR Am J Neuroradiol* 2006;27:1776–81

24. Viallon M, Cuvinciuc V, Delattre B, et al. State-of-the-art MRI techniques in neuroradiology: principles, pitfalls, and clinical applications. *Neuroradiology* 2015;57(5):441-67.

25. Ma C, Li Y, Pan C, et al. High resolution diffusion weighted magnetic resonance imaging of the pancreas using reduced field of view single-shot echo-planar imaging at 3 T. *Magnetic Resonance Imaging* 2014;32(2)125-31.

26. Korn N, Kurhanewicz J, Banerjee S, et al. Reduced-FOV excitation decreases susceptibility artifact in diffusion-weighted MRI with endorectal coil for prostate cancer detection. *Magnetic Resonance Imaging* 2015;33:56–62.

27. Wargo C, Gore J. Localized high-resolution DTI of the human midbrain using single-shot EPI, parallel imaging, and outer-volume suppression at 7T. *Magnetic Resonance Imaging* 2013;31:810–9.

28. Engström M, Skare S. Diffusion-weighted 3D multislab echo planar imaging for high signal-to-noise ratio efficiency and isotropic image resolution. *Magn Reson Med* 2013;70(6):1507–14

29. Grussu F, Schneider T, Zhang H, et al. Neurite orientation dispersion and density imaging of the healthy cervical spinal cord in vivo. *Neuroimage 2015;111:590-601*.

30. Mohammadi S, Freund P, Feiweier T, et al. The impact of post-processing on spinal cord diffusion tensor imaging. *NeuroImage* 2013;70:377-85.

31. Jones D. Diffusion MRI, 1st edition. *Oxford University Press*.

32. Lavdas I, Miquel ME, Aboagye EO, et al. Comparison Between Diffusion-Weighted MRI (DW-MRI) at 1.5 and 3 Tesla: A Phantom Study. *J Magn Reson Imaging* 2014;40(3):682-90.

33. Grech-Sollars M, Hales PW, Clark CA, et al. Multi-centre reproducibility of diffusion MRI parameters for clinical sequences in the brain. *NMR Biomed* 2015;28(4):468-85.

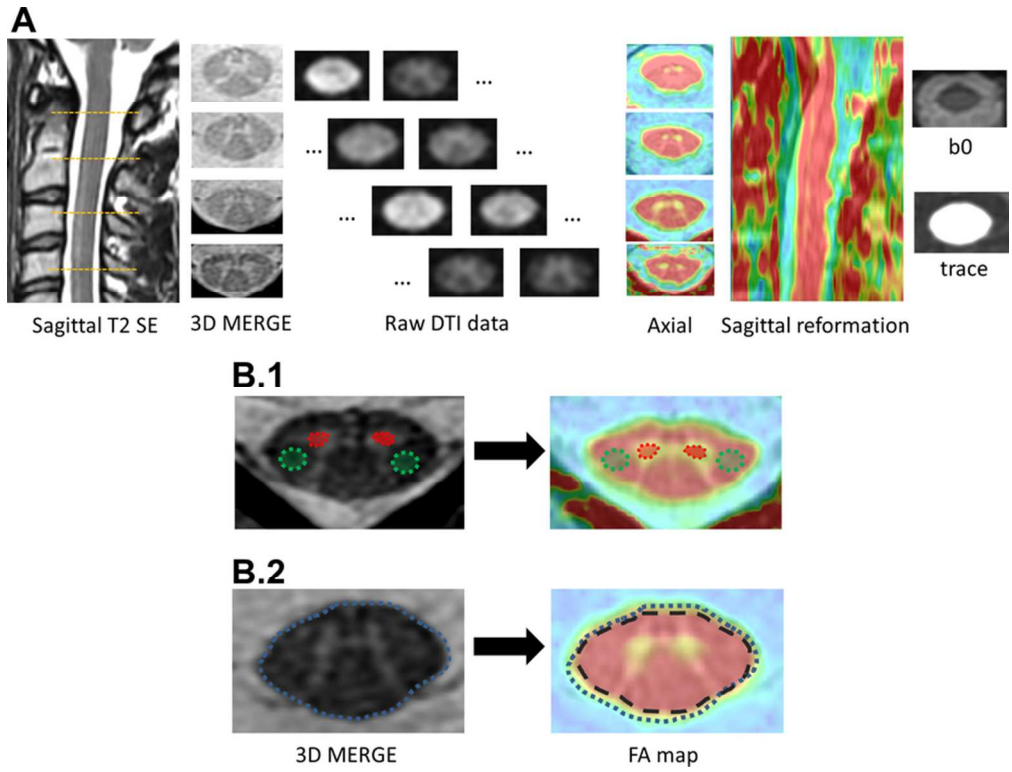

Fig.1: Post-processing pipeline and analyses. A. 4 slices were analyzed in detail: C1, C2, C3 and C4. Raw data diffusion weighted imaging were treated for Eddy current correction prior to generation of DTI parameters. We focused on FA because this parameter is the most commonly used. Fusions of FA and 3D MERGE were created at these four levels as well as reconstruction on sagittal orientation to facilitate the identification of distortions and pixel misregistration. B. ROI positioning: (B.1) ROI were manually delineated on 3D-MERGE, on right and left anterior horn of the cord (red area) for grey matter, and on right and left cortico spinal tract (green area) for white matter, and then propagated on co-registered FA map. (B.2) If needed, ROIs were manually adjusted to account for FA map distortion. Furthermore, because of partial volume effect at the interface between CSF and FA map, ROI of the full section (blue dotted, whose surface corresponded to S(Full Section-merge)) was adjusted to remove the pixels subject to artifact at the periphery of the ROI (black dotted line, whose area corresponded to S(Full Section–FA)).
77x59mm (300 x 300 DPI)

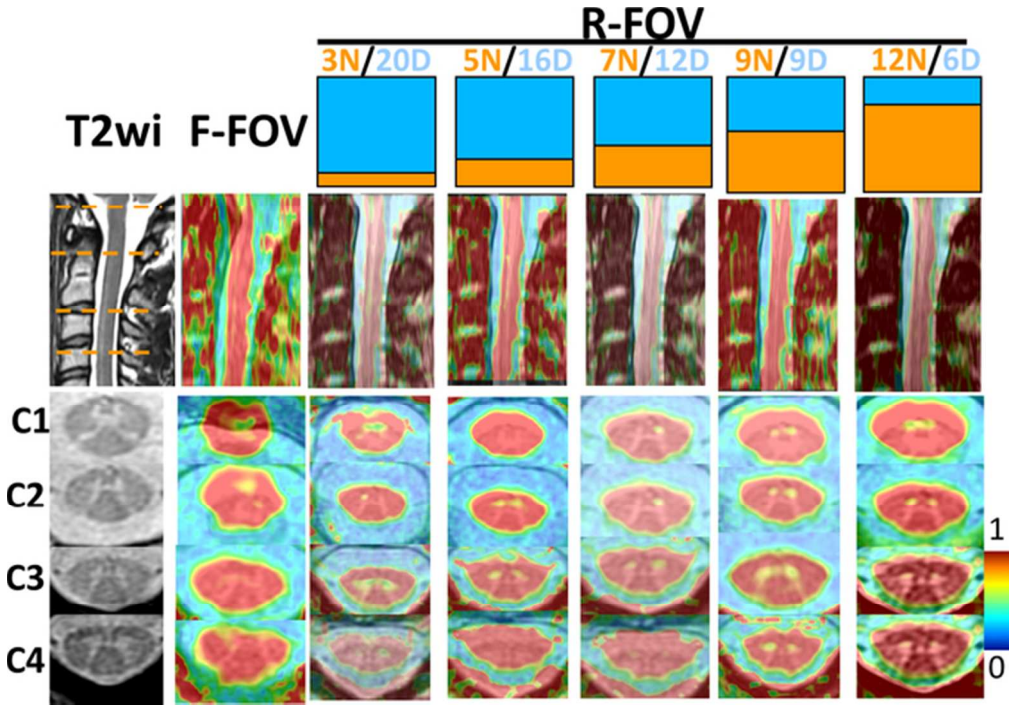

Fig. 2. Examples of MR images available for qualitative analysis. All the images come from the same subject. Cervical levels are located on 3D T2-MERGE and sagittal T2-SE. Fusion of FA – 3D MERGE clearly exhibits that f-FOV DTI and r-FOV 3N/20D are more distorted, more blurred and with less anatomical precision than the other r-FOV.
57x40mm (300 x 300 DPI)

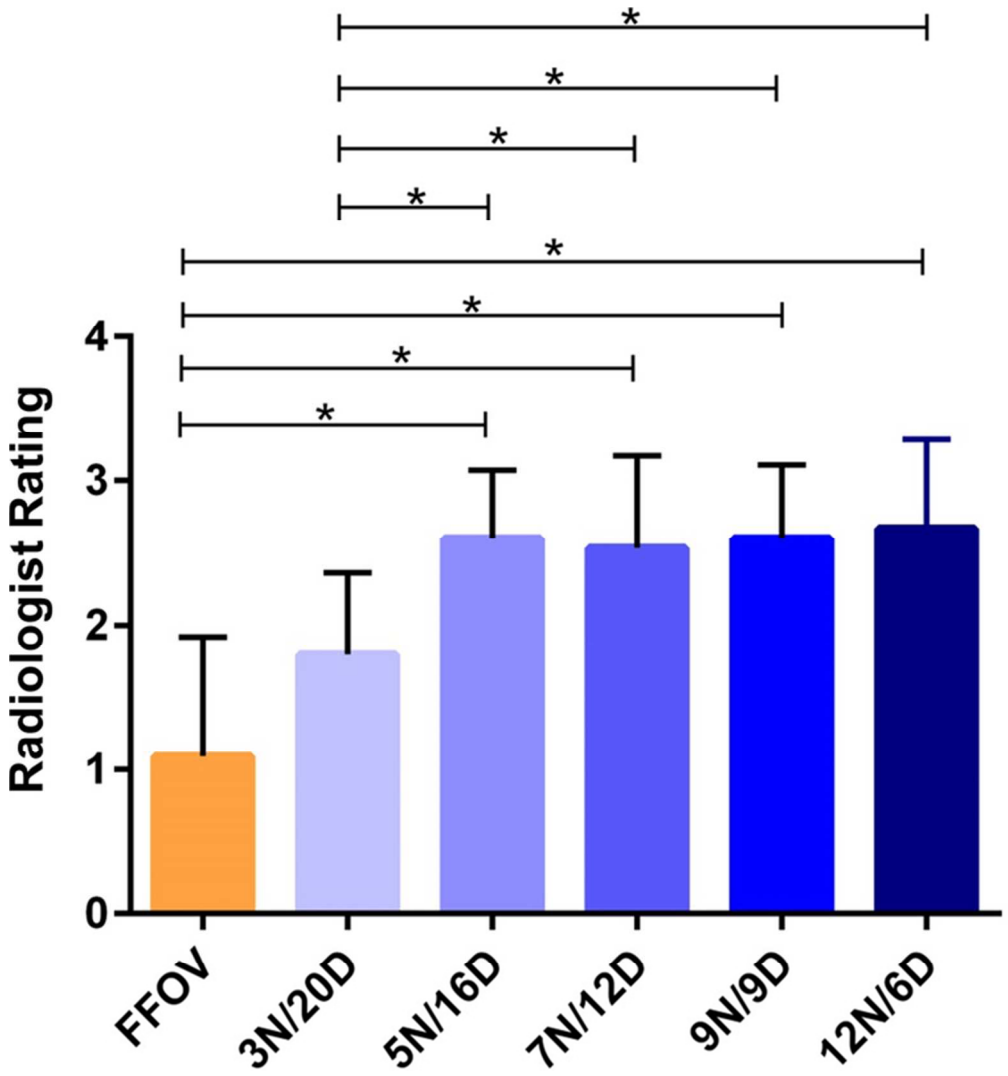

Fig.3: Qualitative analysis. Radiologists attributed a rate to each sequence, for each subject, from 1 (non-diagnostic) to 4 (good). Mean rate ± SD for the sequence are represented. Superimposed black lines indicate which sequences are statistically different with * = $p<0.05$.
64x68mm (300 x 300 DPI)

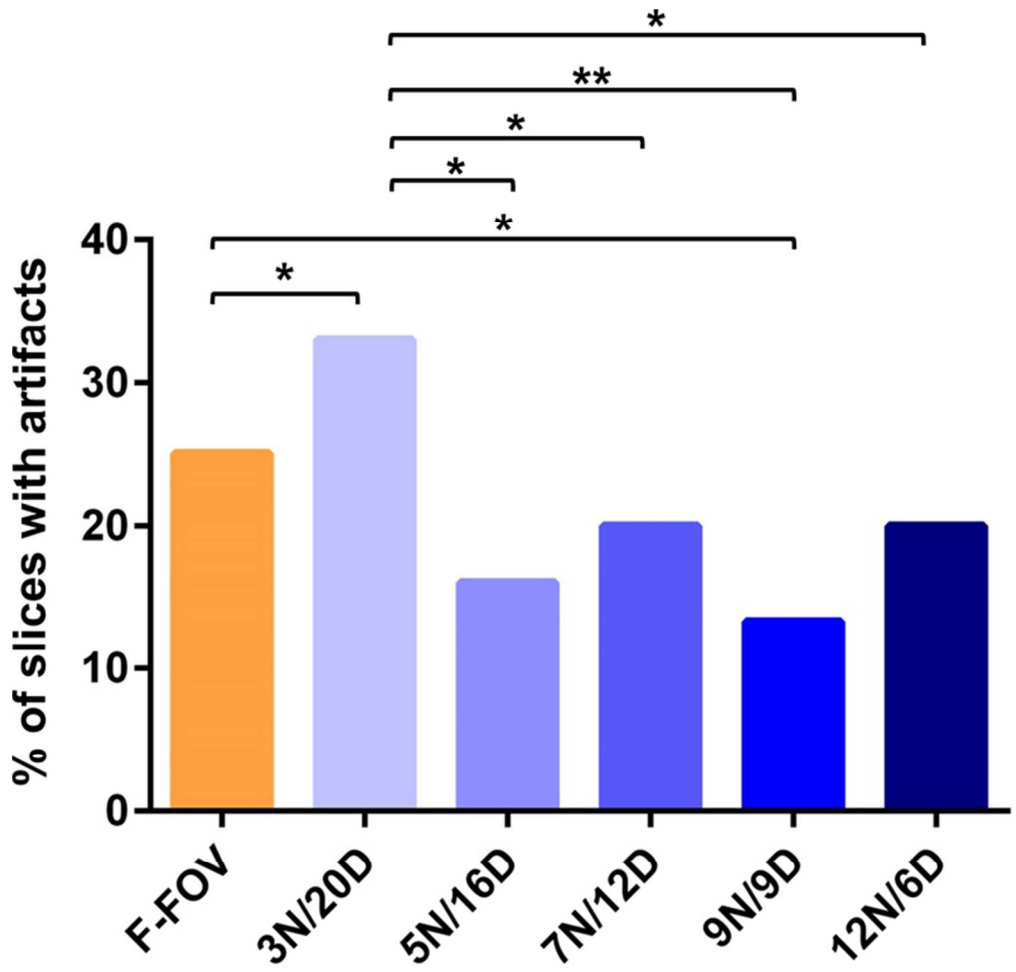

Fig.4: Percentages of slices with artifacts or unusable for DTI analysis, due to susceptibility artifacts or poor SNR. Superimposed black lines indicate which sequences are statistically different with * = $p<0.05$, ** = $p<0.005$.
67x64mm (300 x 300 DPI)

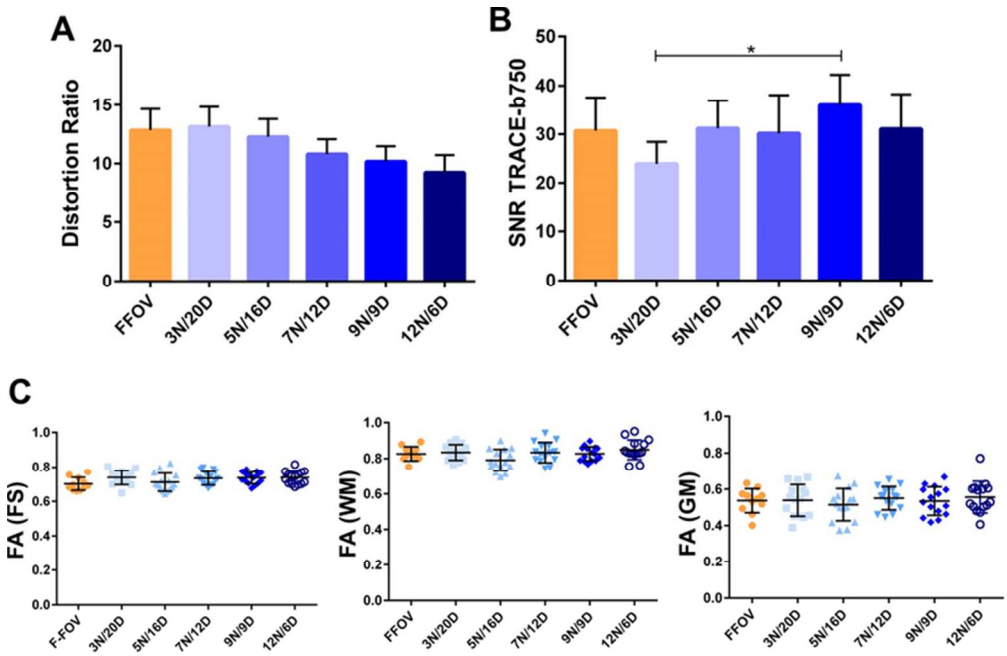

Fig5. Quantitative comparisons on ROI-based analyses. (5.A) exhibits the distortion ratio. (5.B) shows the SNR on the trace image at b=750s/mm². (5.C) aims at representing the dispersion of FA values depending on the DTI sequence and, successively, full section of the spinal cord (FS), WM and GM. Mean rate ± SD for the sequence are represented. Superimposed black lines indicate which sequences are statistically different with * = p<0.05
68x44mm (300 x 300 DPI)

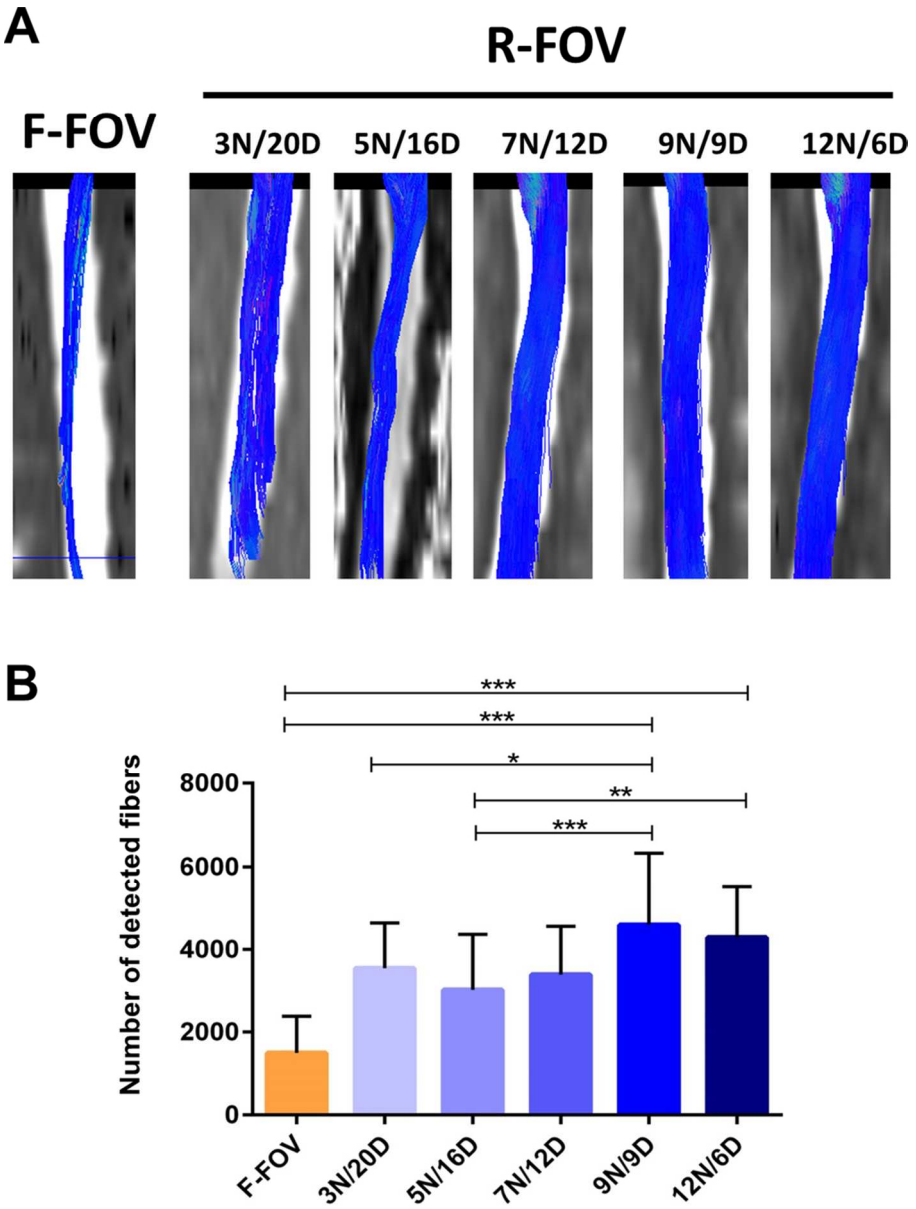

Fig. 6. Tractography-based analyses. (A) exposes the reconstructed tractograms for the whole DTI data set. For each DTI sequence, two similar seed ROIs were placed on anatomical sequence, at C1 and C3 levels and then propagated on diffusion data. Care was taken to exclude abnormal fiber detection (i.e. in the CSF). Qualitatively, r-FOV sequences clearly exhibits better tractograms definition. (B) corresponds to the number of detected fibers between the two seeds. (* = $p<0.05$, ** = $p<0.005$, *** = $p<0.0005$)
87x115mm (300 x 300 DPI)